Entanglement of Trapped-Ion Qubits Separated by 230 Meters

V. Krutyanskiy, M. Galli, V. Krcmarsky, S. Baier, D. A. Fioretto, Y. Pu, A. Mazloom, P. Sekatski, M. Canteri, M. Teller, J. Schupp, J. Bate, M. Meraner, N. Sangouard, B. P. Lanyon, and T. E. Northup

Phys. Rev. Lett. **130**, 050803 — Published 2 February 2023

DOI: 10.1103/PhysRevLett.130.050803

Entanglement of trapped-ion qubits separated by 230 meters

V. Krutyanskiy,[1,2] M. Galli,[2] V. Krcmarsky,[1,2] S. Baier,[2] D. A. Fioretto,[2]
Y. Pu,[2] A. Mazloom,[3] P. Sekatski,[4] M. Canteri,[1,2] M. Teller,[2] J. Schupp,[1,2]
J. Bate,[2] M. Meraner,[1,2] N. Sangouard,[5] B. P. Lanyon,[1,2,*] and T. E. Northup[2]

[1] *Institut für Quantenoptik und Quanteninformation, Osterreichische Akademie der Wissenschaften, Technikerstr. 21a, 6020 Innsbruck, Austria*
[2] *Institut für Experimentalphysik, Universität Innsbruck, Technikerstr. 25, 6020 Innsbruck, Austria*
[3] *Department of Physics, Georgetown University, 37th and O Sts. NW, Washington, DC 20057, USA*
[4] *Department of Applied Physics, University of Geneva, 1211 Geneva, Switzerland*
[5] *Institut de Physique Théorique, Université Paris-Saclay, CEA, CNRS, 91191 Gif-sur-Yvette, France*

(Dated: December 20, 2022)

We report on an elementary quantum network of two atomic ions separated by 230 m. The ions are trapped in different buildings and connected with 520(2) m of optical fiber. At each network node, the electronic state of an ion is entangled with the polarization state of a single cavity photon; subsequent to interference of the photons at a beamsplitter, photon detection heralds entanglement between the two ions. Fidelities of up to $(88.0+2.2-4.7)\%$ are achieved with respect to a maximally entangled Bell state, with a success probability of 4×10^{-5}. We analyze the routes to improve these metrics, paving the way for long-distance networks of entangled quantum processors.

The realization of quantum networks [1, 2] that link cities and countries would open up powerful new applications in information security [3], distributed computing [4, 5], precision sensing [6, 7] and timekeeping [8]. These applications require distributed quantum network nodes that, first, can be entangled via the exchange of photons over long distances and, second, can store and process quantum information encoded in registers of qubits. A handful of experiments have demonstrated remote entanglement of two quantum-logic-capable qubits, including ions in linear Paul traps [9, 10], optically trapped neutral atoms [11, 12], color centers in diamond [13], quantum dots [14, 15] and superconducting qubits [16]; furthermore, three-node entanglement of color centers was recently achieved [17]. These elementary networks have been extended to entangle quantum systems in separate buildings: two diamond color centers 1.3 km apart [18] and two neutral atoms 400 m apart [19, 20].

Quantum network nodes based on trapped ions [21] promise high-fidelity quantum-gate operations on registers of tens of qubits [22, 23], coherence times exceeding one hour [24], efficient interfacing with telecom-wavelength photons [25, 26] and precision sensing and metrology [27–29]. Building on the first demonstration of remote-ion entanglement [9], significant improvements in both rate and fidelity [10, 30] have recently enabled device-independent quantum key distribution [31] and enhanced timekeeping [32], and a multispecies node has been demonstrated [33]. Remote entanglement of trapped ions more than a few meters apart has not previously been reported.

In this Letter, we report on the entanglement of two trapped ions separated by 230 m. The two ions are in separate buildings, connected via 520(2) m of optical fiber, and controlled by independent lasers and electronics. Their entanglement is heralded by the coincident detection of two infrared photons that travel through the fiber. In contrast to implementations based on spontaneous emission [9, 10, 12–15, 17, 19, 20, 30, 33], our photon generation method is based on a cavity-mediated Raman process providing tunable entangled states [34] and high efficiency [35], which are advantageous for establishing long-distance entanglement [36]. Remote ion–ion entanglement is characterized by quantum state tomography and analyzed for a range of time windows for coincident detection. A detailed model is developed that captures the observed trade-off between the fidelity of remote entanglement and the heralding efficiency and shows how significant improvements can be made in the future.

Each node in our quantum network (Fig. 1(a),(b)) consists of a single $^{40}Ca^{+}$ atom confined in a linear Paul trap and coupled to a 20 mm cavity for photon collection at 854 nm. A photon is generated at each node via a bichromatic cavity-mediated Raman transition (Fig. 1(c)) [34]. Here, a Raman laser pulse applied to the ion ideally generates the maximally entangled ion–photon state $|\psi_k\rangle = 1/\sqrt{2}\left(|\mathrm{DV}\rangle + e^{i\theta_k}|\mathrm{D'H}\rangle\right)$, where $|\mathrm{D}\rangle$ and $|\mathrm{D'}\rangle$ are the respective Zeeman states $|3^2\mathrm{D}_{5/2}, m_j=-5/2\rangle$ and $|3^2\mathrm{D}_{5/2}, m_j=-3/2\rangle$, $|\mathrm{V}\rangle$ and $|\mathrm{H}\rangle$ are the vertical and horizontal polarization components of a photon emitted into the cavity vacuum mode, and θ_k is a phase set at node $k\in\{\mathrm{A},\mathrm{B}\}$. The photon exits the cavity and is coupled into single-mode optical fiber. Two photons, one from each node, arrive at a photonic Bell-state measurement (PBSM) setup, where their spatial modes are overlapped on a balanced beamsplitter [37–39]. Coincident detection of orthogonally polarized photons ideally heralds the maximally entangled ion–ion states

$$|\Psi^{\pm}\rangle = 1/\sqrt{2}\left(|\mathrm{D_A D'_B}\rangle \pm e^{i\phi}\,|\mathrm{D'_A D_B}\rangle\right), \qquad (1)$$

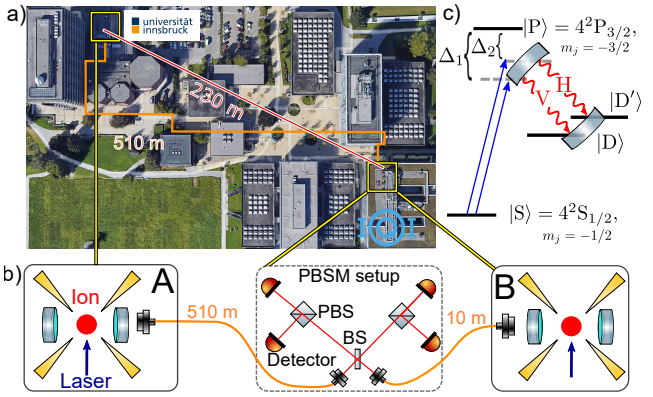

FIG. 1. The two-node quantum network. a) Satellite image (Google Earth, image: Landsat / Copernicus). Nodes A and B are located in separate buildings, connected via a 520(2) m optical-fiber link and have a 230 m line of sight separation. b) Nodes consist of an ion, a linear Paul trap (four yellow electrodes) and a cavity comprised of two mirrors. The photonic Bell-state measurement (PBSM) setup contains a beam splitter (BS), polarizing beam splitters (PBS) and photon detectors. c) Energy-level diagram for $^{40}Ca^+$. When an ion is in state $|S\rangle$ and no photons are in the cavity, a laser pulse containing two tones generates the ion–photon entangled state $1/\sqrt{2}\left(|\mathrm{DV}\rangle + e^{i\theta}|\mathrm{D'H}\rangle\right)$, where $|\mathrm{V}\rangle$ and $|\mathrm{H}\rangle$ are the polarization components of a cavity photon and θ is a phase [34]. The frequency difference $\Delta_2 - \Delta_1$ is equal to the one between $|\mathrm{D'}\rangle = 3^2\mathrm{D}_{5/2}, m_j = -3/2$ and $|\mathrm{D}\rangle = 3^2\mathrm{D}_{5/2}, m_j = -5/2$.

with phase $\phi = \theta_\mathrm{A} - \theta_\mathrm{B}$, where subscripts indicate the ion node. The state $|\Psi^+\rangle$ is obtained if the two coincident detection events occur in the same output mode of the beamsplitter, while $|\Psi^-\rangle$ is obtained if coincident detection occurs in opposite output modes.

Which-path information for the two photons can be erased in the PBSM, which requires both temporal and spectral indistinguishability of the photon wavepackets. Each node has control software and hardware that executes a finite-length and node-specific remote entanglement sequence: a list of operations to perform. Each control system is referenced to its own 10 MHz GPS clock source. Temporal synchronization of the two sequences to within a 30 ns jitter is achieved via a handshake between the control systems at the start of each sequence. The handshake signal is sent over a dedicated optical fiber in a fiber bundle connecting the two labs, which also contains the fiber for single-photon distribution. Offsets in the arrival times of temporal photon wavepackets at the PBSM, e.g., due to optical path differences, are compensated for by introducing sequence delays.

Spectral indistinguishability of the photons requires matching the resonant frequencies of the remote cavities. This is achieved via periodic calibration at 20 min intervals: 854 nm laser light that is resonant with the cavity at Node A is sent to Node B over a third fiber in the bundle, and the length of the Node B cavity is adjusted until

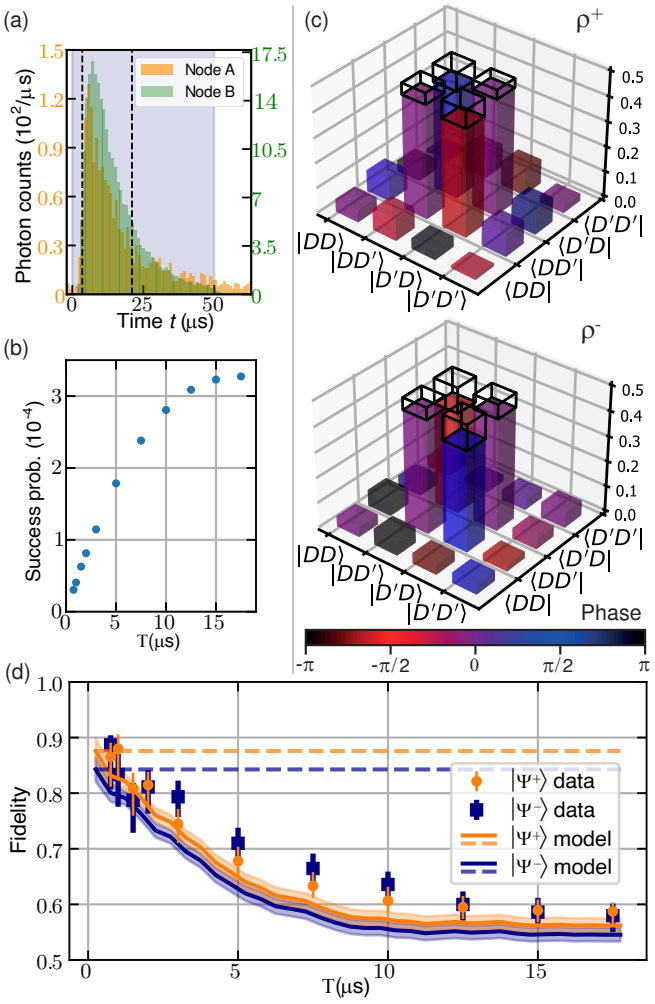

FIG. 2. Entanglement between ion qubits. (a) Single-photon wavepackets measured at each node in a separate calibration experiment. Shown are histograms of photon counts per 1 μs time bin for ion-entangled photons from Node A only (orange) and Node B only (green). The gray region indicates when the Raman laser pulse is on. The dashed black lines indicate the window within which coincidence events are evaluated during entanglement experiments. (b) Success probability for a coincidence event heralding either $|\psi^+\rangle$ or $|\psi^-\rangle$ to occur as a function of T. (c) Experimentally reconstructed density matrices $\rho^+(T)$ and $\rho^-(T)$, for $T = 1\,\mu\mathrm{s}$. Bar heights indicate amplitudes of matrix entries; colors indicate phases. Amplitudes of the entries for $|\Psi^\pm\rangle\langle\Psi^\pm|$ are outlined for comparison. (d) Fidelity $F^\pm$ as a function of T. Markers indicate measured values; error bars correspond to one standard deviation. Solid lines show an empirical model discussed in the main text, with shaded regions indicating uncertainties. Dashed lines show a partial model omitting photon distinguishability.

it is resonant with this light. Also at 20 min intervals, the polarization rotation of the fiber that carries single photons is characterized and corrected for [40].

The remote entanglement sequences at each node contain a loop in which up to 20 attempts are made to establish ion–ion entanglement. Each attempt contains 0.3 ms

of state initialization, via Doppler cooling and optical pumping, followed by a Raman laser pulse of 50 µs to generate a photon. In the case of coincident detection of orthogonally polarized photons within a 50 µs window that encompasses the single-photon wavepackets, the sequence exits the loop, and the ion qubits are measured. Ion-qubit measurement consists of laser-driven single-qubit rotations to set the measurement basis, followed by state detection via electron shelving for 1.5 ms, at which point the sequence is concluded.

The remote ion–ion state is characterized via quantum state tomography, for which the sequence is repeated for all nine combinations of the Pauli measurement bases for two ion qubits [41]. Tomographic reconstruction, via the maximum likelihood technique, yields the density matrices $\rho^{\pm}(T)$, where ρ^{+} and ρ^{-} are reconstructed for the coincidences corresponding to ideally $|\Psi^{+}\rangle$ and $|\Psi^{-}\rangle$, respectively, and T is the maximum time difference for which entanglement is heralded between coincident photons. A fidelity $F^{\pm}(T) \equiv \langle\Psi^{\pm}|\rho^{\pm}(T)|\Psi^{\pm}\rangle > 0.5$ proves entanglement of the remote ions. Uncertainties for $F^{\pm}(T)$ and for all quantities derived from the density matrices are obtained via Monte Carlo resampling [40].

Data were acquired over seven hours, including interspersed calibrations. For each basis measurement setting, 17 min of data were acquired on average. In total, 13 656 928 attempts were made to generate remote entanglement, resulting in 4470 coincidence events within the interval $[t = 5.5\,\mu\text{s}, t = 23\,\mu\text{s}]$ (Fig. 2(a)), corresponding to a 0.033 % probability of two-photon coincidence per attempt, which we define as the success probability. Here $t = 0$ indicates the start of the 50 µs detection window, and the narrower interval has been chosen to improve signal to noise. The remote entanglement rate during the data acquisition time is thus $0.49\,\text{s}^{-1}$. The fidelities of the reconstructed states are $F^{+}(17.5\,\mu\text{s}) = (58.7{+}1.7{-}2.1)\%$ and $F^{-}(17.5\,\mu\text{s}) = (58.0{+}2.0{-}2.9)\%$, where $T = 17.5\,\mu\text{s}$ corresponds to all possible coincidences within the 17.5 µs window.

When we take a subset of the data corresponding to coincidences separated by smaller values of T, entangled ion–ion states are generated with higher fidelity, at the cost of a lower success probability (Fig. 2(b)). The density matrices shown in Fig. 2(c) correspond to $T = 1\,\mu\text{s}$, for which we recorded 555 coincidence events, that is, a remote entanglement rate of $3.5\,\text{min}^{-1}$. The fidelities of the reconstructed states are $F^{+}(1\,\mu\text{s}) = (88.0 + 2.2 - 4.7)\%$ and $F^{-}(1\,\mu\text{s}) = (83.3 + 3.3 - 6.4)\%$. We optimize $F^{\pm}$ over the phase ϕ in Eq. 1 because we did not determine θ_A and θ_B independently; this optimization yields $\phi = 82.2°$. We then fix this value of ϕ for all subsequent data points. In Fig. 2(d), we plot the measured fidelities for values of T between 0.75 µs and 17.5 µs.

A decrease in fidelity as T increases is to be expected: for example, spontaneous emission during the Raman process provides information on which ion generated which cavity photon [42–44], that is, scattering introduces which-path information. To predict our experimentally determined fidelities, we have developed an empirical model for the ion–ion density matrix heralded by two-photon detection. The model contains photon distinguishability [45] along with two other sources of infidelity: detector background counts and imperfect ion–photon entanglement. The values of $F^{\pm}(T)$ calculated using this density-matrix model are plotted in Fig. 2(d) along with the measured values. We will first explain the contributions of photon distinguishability to this model and will afterwards discuss the other sources of infidelity [40].

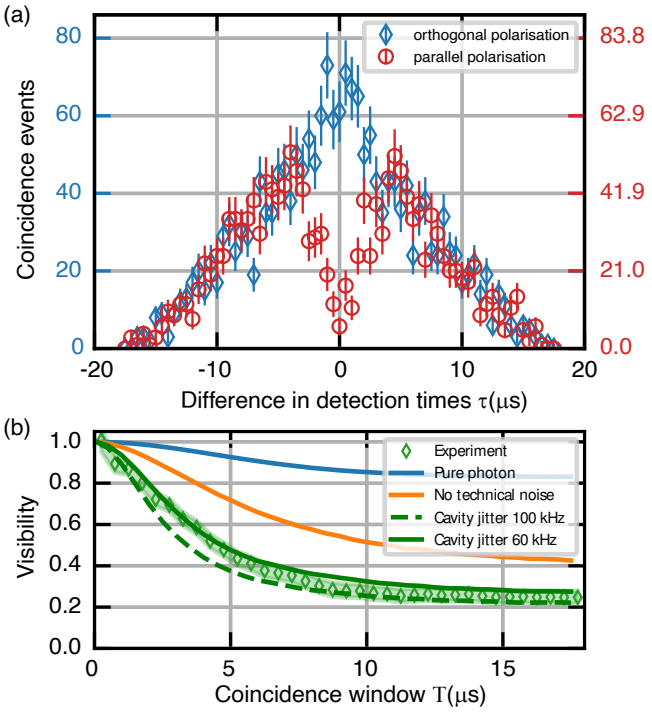

FIG. 3. (a) Number of coincidences recorded for orthogonal (blue) and parallel (red) polarization projections of photons from Nodes A and B, for the same data set as in Fig. 2, where the axes are scaled by the ratio of detector efficiencies. Data are plotted as a function of the time difference τ between photon detection events, binned in 0.5 µs intervals. Error bars indicate Poissonian statistics. (b) Diamonds show the two-photon interference visibility calculated from the coincidence data after correction for background counts and detector efficiencies, using Eq. 2. The shaded region indicates the propagation of Poissonian uncertainties. Lines show a master-equation model discussed in the main text.

To account for photon distinguishability, we employ a two-qubit dephasing channel, which reduces the off-diagonal elements of the ideal density matrices $|\Psi^{\pm}\rangle\langle\Psi^{\pm}|$ [40]. The probability for dephasing in the channel is parameterized by the Hong-Ou-Mandel (HOM) interference visibility, which provides direct information about photon indistinguishability [46]. For unit visibility, no dephasing occurs, while for a visibil-

ity of zero, all off-diagonal matrix elements are zero.

The HOM visibility is extracted from the photon coincidence data by sorting all events in which photons are detected at opposite ports of the balanced beamsplitter into two sets: coincidences with identical polarization and with orthogonal polarization. Photons with identical polarization will exit the balanced beamsplitter at the same output port if they are otherwise indistinguishable, generating a HOM dip in coincidence counts at the two output ports [47]. Orthogonally polarized photons are distinguishable and thus exhibit no HOM effect; their cross-correlation function allows us to normalize the HOM dip and thereby to calculate the interference visibility. In Fig. 3(a), the number of coincidence events is plotted for both sets of data as a function of the time difference τ between photon detection events, for a time bin $\delta = 0.5\,\mu s$. The HOM dip at $\tau = 0$ can be clearly observed. The interference visibility is then obtained from the data of Fig. 3(a) via the following procedure: First, the number of expected coincidences between photons and detector background counts is subtracted from the number of measured coincidences for each time bin. Next, the data sets are corrected for the detector efficiencies, which have been independently measured [40]. We define $N_{\parallel,k\delta}$ and $N_{\perp,k\delta}$ as the corrected numbers of coincidences for the time bin centered at $\tau = k\delta$ for $k \in \mathbb{Z}$, where the symbols $\parallel$ and $\perp$ indicate identical and orthogonal photon polarization, respectively. Finally, the interference visibility is calculated as a function of the coincidence window T:

$$V(T) = 1 - \frac{\sum_{(-T+\delta/2)\leq k\delta\leq(T-\delta/2)} N_{\parallel,k\delta}}{\sum_{(-T+\delta/2)\leq k\delta\leq(T-\delta/2)} N_{\perp,k\delta}} \qquad (2)$$

In Fig. 3(b), $V(T)$ is plotted for coincidence windows up to 17.5 µs, as in Fig. 2(d), and for 0.5 µs time bins. The maximum visibility corresponds to $101(6)\,\%$ for $T = 0.25\,\mu s$; this value is above $100\,\%$ because the background-corrected value for $N_{\parallel,k\delta}$ is negative, while consistent with zero within one standard deviation.

Our empirical model also includes detector background counts and imperfect ion–photon entanglement. For background counts, we use a white-noise channel based on the independently measured count rates of the four detectors. For ion–photon entanglement, we assume that imperfections translate as a two-qubit depolarizing channel on the ion–ion state [40]. Ion–photon entanglement was characterized in a calibration measurement at each node via quantum state tomography immediately prior to ion–ion entanglement, and fidelities of $(92.9+0.4-0.5)\%$ and $(95.5+0.6-0.9)\%$ with respect to a maximally entangled state were obtained at Nodes A and B, respectively.

The empirical model is used to calculate the theoretical fidelities of Fig. 2(d): The solid lines are calculated from the full model, taking into account all three sources of infidelity, while the dashed lines are calculated when photon distinguishability is excluded from the model. Different values are predicted for F^+ and F^- due to the use of superconducting nanowire detectors at two of the four beamsplitter outputs, which have lower dark-count rates than the single-photon-counting modules at the other two outputs. Based on the agreement between measured and modeled fidelities in Fig. 2(d), we conclude that the model captures the relevant properties of our setup and that the observed decline in fidelity as a function of T is due to the corresponding decline in visibility.

For insight into how, in the future, visibility could be maintained for larger coincidence windows—thereby increasing the probability to establish remote entanglement with a given fidelity—we have developed a master-equation model based on that of Ref. [44]. This model considers three independently estimated noise processes that result in non-transform-limited (and therefore distinguishable) photons at each node: frequency jitter of the Node A cavity by $60 - 100\,\mathrm{kHz}$, Raman-laser phase noise, and spontaneous emission. We refer to the first two of these processes as technical noise. All parameter values used in the model are statistically consistent with independent estimates and determined via comparison of the model to measured single-photon wavepackets [40]. The predicted visibility is plotted in Fig. 3(b): green lines indicate the full model, including upper and lower estimates of the frequency jitter. It can be seen that the model is consistent with the visibility data.

We now look to the master-equation model to understand the impact of future improvements. Setting the technical noise contributions of cavity jitter and laser phase noise to zero, as shown in orange in Fig. 3(b), improves the model visibility. In addition, selecting only those ion–photon entanglement events for which no spontaneous emission occurs, corresponding to transform-limited or 'pure' photons, leads to the most significant improvement in the model visibility (blue line). The remaining visibility imperfections are due to mismatch between the temporal wavepackets of the transform-limited photons produced at each node [40].

With regards to the technical noise contributions, we expect to suppress both cavity jitter and laser phase noise to negligible levels by improving the lock electronics and the passive cavity used as a laser reference at Node A. Meanwhile, temporal wavepacket mismatch can be addressed through amplitude shaping of the Raman laser pulse [48]. It is spontaneous emission that poses the most significant challenge. Using our existing setup, multi-ion superradiant states can be harnessed to boost the fraction of photons generated without prior spontaneous decay [42]; in future ion–cavity nodes, further gains can be obtained through judicious choice of the mirror properties and cavity geometry [35]. All these steps will increase the probability to generate transform-limited photons in each entanglement attempt. Additional steps can be taken to increase the attempt rate, namely, in the

short term, implementing more efficient cooling and state detection protocols, and in the long term, coupling ions to fiber-based cavities with stronger coherent coupling and faster decay rates [49]. It is notable that the success probabilities shown in Fig. 2(b) are comparable to those achieved over a few meters in Ref. [10], and that in future long-distance networks limited by photon travel time, it will be success probabilities that determine entanglement rates [36].

In conclusion, we have verified entanglement over the longest trapped-ion network to date, with fidelities up to $(88.0 + 2.2 - 4.7)\%$ with respect to a maximally entangled state. A trade-off between fidelity and coincidence-window length was explained with the help of two models: an empirical model for the two-ion density matrix and a master-equation model to predict the interference visibility. Based on these models, we anticipate that we will be able to obtain significantly higher rates across this cavity-mediated network while maintaining high fidelities. Furthermore, efficient, low-noise and entanglement-preserving telecom wavelength conversion of the 854 nm photons used in the present work has been achieved [25, 26], opening the possibility to extend the quantum channel to hundreds of kilometers. While the experiments presented here relied on just one ion at each node, a particular strength of the trapped-ion platform is the capability for quantum-information processing with dozens of addressed qubits in a single trap [22, 23] and fidelities sufficient for fault-tolerant gate operations and error correction [50, 51]. This capability provides a route to robust logical qubit encodings at network nodes [52], separate communication and information processing functionalities within each node [5, 21], and quantum repeaters requiring Bell state measurements and either purification or error correction [53].

Datasets are available online [54].

This work was supported by the European Union's Horizon 2020 research and innovation program under grant agreement No. 820445 and project name "Quantum Internet Alliance," by Projects F 7109 and Y 849 of the Austrian Science Fund (FWF), and by the U.S. Army Research Laboratory's Center for Distributed Quantum Information under Cooperative Agreement Number W911NF-15-2-0060. We acknowledge funding for S.B. by an FWF Erwin Schrödinger fellowship (No. J 4229), for V. Krutyanskiy by the Erwin Schrödinger Center for Quantum Science & Technology (ESQ) Discovery Programme, for B.P.L. by the CIFAR Quantum Information Science Program of Canada, for A.M. by the U.S. National Science Foundation under Grant No. PHY-1915130, for N.S. by the Commissariat à l'Energie Atomique et aux Energies Alternatives (CEA), and for M.T. by the Early Stage Funding Program of the Vice-Rectorate for Research of the University of Innsbruck.

M.G. and V. Krutyanskiy contributed equally to this work. S.B., D.F., M.G., V. Krcmarsky, V. Krutyanskiy, M.M., Y.P., and J.S. contributed to the experimental setup. S.B., J.B., M.C., D.F., M.G., V. Krcmarsky, V. Krutyanskiy, Y.P., and M.T. took data. S.B., M.C., M.G., and V. Krutyanskiy analyzed data. S.B., J.B., D.F., V. Krcmarsky, V. Krutyanskiy, A.M., Y.P., N.S., J.S., and P.S. performed theoretical modeling. B.P.L. and T.E.N. wrote the main text, with contributions from all authors. The project was conceived and supervised by B.P.L. and T.E.N.

* Correspondence should be send to ben.lanyon@uibk.ac.at

[1] H. J. Kimble, The quantum internet, Nature **453**, 1023 (2008).
[2] S. Wehner, D. Elkouss, and R. Hanson, Quantum internet: A vision for the road ahead, Science **362** (2018).
[3] S. Pirandola, U. L. Andersen, L. Banchi, M. Berta, D. Bunandar, R. Colbeck, D. Englund, T. Gehring, C. Lupo, C. Ottaviani, J. L. Pereira, M. Razavi, J. S. Shaari, M. Tomamichel, V. C. Usenko, G. Vallone, P. Villoresi, and P. Wallden, Advances in quantum cryptography, Adv. Opt. Photon. **12**, 1012 (2020).
[4] L. Jiang, J. M. Taylor, A. S. Sørensen, and M. D. Lukin, Distributed quantum computation based on small quantum registers, Phys. Rev. A **76**, 062323 (2007).
[5] C. Monroe, R. Raussendorf, A. Ruthven, K. R. Brown, P. Maunz, L.-M. Duan, and J. Kim, Large-scale modular quantum-computer architecture with atomic memory and photonic interconnects, Phys. Rev. A **89**, 022317 (2014).
[6] T. J. Proctor, P. A. Knott, and J. A. Dunningham, Multiparameter estimation in networked quantum sensors, Phys. Rev. Lett. **120**, 080501 (2018).
[7] P. Sekatski, S. Wölk, and W. Dür, Optimal distributed sensing in noisy environments, Phys. Rev. Research **2**, 023052 (2020).
[8] P. Kómár, E. M. Kessler, M. Bishof, L. Jiang, A. S. Sørensen, J. Ye, and M. D. Lukin, A quantum network of clocks, Nat. Phys. **10**, 582 (2014).
[9] D. L. Moehring, P. Maunz, S. Olmschenk, K. C. Younge, D. N. Matsukevich, L. M. Duan, and C. Monroe, Entanglement of single-atom quantum bits at a distance, Nature **449**, 68 (2007).
[10] L. J. Stephenson, D. P. Nadlinger, B. C. Nichol, S. An, P. Drmota, T. G. Ballance, K. Thirumalai, J. F. Goodwin, D. M. Lucas, and C. J. Ballance, High-rate, high-fidelity entanglement of qubits across an elementary quantum network, Phys. Rev. Lett. **124**, 110501 (2020).
[11] S. Ritter, C. Nölleke, C. Hahn, A. Reiserer, A. Neuzner, M. Uphoff, M. Mücke, E. Figueroa, J. Bochmann, and G. Rempe, An elementary quantum network of single atoms in optical cavities, Nature **484**, 195 (2012).
[12] J. Hofmann, M. Krug, N. Ortegel, L. Gérard, M. Weber, W. Rosenfeld, and H. Weinfurter, Heralded entanglement between widely separated atoms, Science **337**, 72 (2012).
[13] H. Bernien, B. Hensen, W. Pfaff, G. Koolstra, M. Blok, L. Robledo, T. Taminiau, M. Markham, D. Twitchen, L. Childress, and R. Hanson, Heralded entanglement between solid-state qubits separated by three metres, Na-

ture **497**, 86 (2013).
[14] A. Delteil, Z. Sun, W.-b. Gao, E. Togan, S. Faelt, and A. Imamoğlu, Generation of heralded entanglement between distant hole spins, Nat. Phys. **12**, 218 (2016).
[15] R. Stockill, M. J. Stanley, L. Huthmacher, E. Clarke, M. Hugues, A. J. Miller, C. Matthiesen, C. Le Gall, and M. Atatüre, Phase-tuned entangled state generation between distant spin qubits, Phys. Rev. Lett. **119**, 010503 (2017).
[16] P. Magnard, S. Storz, P. Kurpiers, J. Schär, F. Marxer, J. Lütolf, T. Walter, J.-C. Besse, M. Gabureac, K. Reuer, A. Akin, B. Royer, A. Blais, and A. Wallraff, Microwave quantum link between superconducting circuits housed in spatially separated cryogenic systems, Phys. Rev. Lett. **125**, 260502 (2020).
[17] M. Pompili, S. L. N. Hermans, S. Baier, H. K. C. Beukers, P. C. Humphreys, R. N. Schouten, R. F. L. Vermeulen, M. J. Tiggelman, L. dos Santos Martins, B. Dirkse, S. Wehner, and R. Hanson, Realization of a multinode quantum network of remote solid-state qubits, Science **372**, 259 (2021).
[18] B. Hensen, H. Bernien, A. E. Dréau, A. Reiserer, N. Kalb, M. S. Blok, J. Ruitenberg, R. F. Vermeulen, R. N. Schouten, C. Abellán, *et al.*, Loophole-free Bell inequality violation using electron spins separated by 1.3 kilometres, Nature **526**, 682 (2015).
[19] W. Zhang, T. van Leent, K. Redeker, R. Garthoff, R. Schwonnek, F. Fertig, S. Eppelt, W. Rosenfeld, V. Scarani, C. C.-W. Lim, and H. Weinfurter, A device-independent quantum key distribution system for distant users, Nature **607**, 687 (2022).
[20] T. van Leent, M. Bock, F. Fertig, R. Garthoff, S. Eppelt, Y. Zhou, P. Malik, M. Seubert, T. Bauer, W. Rosenfeld, W. Zhang, C. Becher, and H. Weinfurter, Entangling single atoms over 33 km telecom fibre, Nature **607**, 69 (2022).
[21] L.-M. Duan and C. Monroe, Colloquium: Quantum networks with trapped ions, Rev. Mod. Phys. **82**, 1209 (2010).
[22] C. D. Bruzewicz, J. Chiaverini, R. McConnell, and J. M. Sage, Trapped-ion quantum computing: Progress and challenges, Appl. Phys. Rev. **6**, 021314 (2019).
[23] N. Friis, O. Marty, C. Maier, C. Hempel, M. Holzäpfel, P. Jurcevic, M. B. Plenio, M. Huber, C. Roos, R. Blatt, and B. Lanyon, Observation of entangled states of a fully controlled 20-qubit system, Phys. Rev. X **8**, 021012 (2018).
[24] Y. Wang, M. Um, J. Zhang, S. An, M. Lyu, J.-N. Zhang, L.-M. Duan, D. Yum, and K. Kim, Single-qubit quantum memory exceeding ten-minute coherence time, Nat. Photonics **11**, 646 (2017).
[25] M. Bock, P. Eich, S. Kucera, M. Kreis, A. Lenhard, C. Becher, and J. Eschner, High-fidelity entanglement between a trapped ion and a telecom photon via quantum frequency conversion, Nat. Commun. **9**, 1998 (2018).
[26] V. Krutyanskiy, M. Meraner, J. Schupp, V. Krcmarsky, H. Hainzer, and B. P. Lanyon, Light-matter entanglement over 50 km of optical fibre, npj Quantum Inf. **5**, 72 (2019).
[27] S. M. Brewer, J.-S. Chen, A. M. Hankin, E. R. Clements, C. W. Chou, D. J. Wineland, D. B. Hume, and D. R. Leibrandt, $^{27}Al^{+}$ quantum-logic clock with a systematic uncertainty below 10^{-18}, Phys. Rev. Lett. **123**, 033201 (2019).
[28] K. A. Gilmore, M. Affolter, R. J. Lewis-Swan, D. Barberena, E. Jordan, A. M. Rey, and J. J. Bollinger, Quantum-enhanced sensing of displacements and electric fields with two-dimensional trapped-ion crystals, Science **373**, 673 (2021).
[29] C. D. Marciniak, T. Feldker, I. Pogorelov, R. Kaubruegger, D. V. Vasilyev, R. van Bijnen, P. Schindler, P. Zoller, R. Blatt, and T. Monz, Optimal metrology with programmable quantum sensors, Nature **603**, 604 (2022).
[30] D. Hucul, I. V. Inlek, G. Vittorini, C. Crocker, S. Debnath, S. M. Clark, and C. Monroe, Modular entanglement of atomic qubits using photons and phonons, Nat. Phys. **11**, 37 (2015).
[31] D. P. Nadlinger, P. Drmota, B. C. Nichol, G. Araneda, D. Main, R. Srinivas, D. M. Lucas, C. J. Ballance, K. Ivanov, E. Y.-Z. Tan, P. Sekatski, R. L. Urbanke, R. Renner, N. Sangouard, and J.-D. Bancal, Device-independent quantum key distribution (2021), arxiv:2109.14600.
[32] B. C. Nichol, R. Srinivas, D. P. Nadlinger, P. Drmota, D. Main, G. Araneda, C. J. Ballance, and D. M. Lucas, A quantum network of entangled optical atomic clocks (2021), arxiv:2111.10336.
[33] I. V. Inlek, C. Crocker, M. Lichtman, K. Sosnova, and C. Monroe, Multispecies trapped-ion node for quantum networking, Phys. Rev. Lett. **118**, 250502 (2017).
[34] A. Stute, B. Casabone, P. Schindler, T. Monz, P. O. Schmidt, B. Brandstätter, T. E. Northup, and R. Blatt, Tunable ion-photon entanglement in an optical cavity, Nature **485**, 482 (2012).
[35] J. Schupp, V. Krcmarsky, V. Krutyanskiy, M. Meraner, T. Northup, and B. Lanyon, Interface between trapped-ion qubits and traveling photons with close-to-optimal efficiency, PRX Quantum **2**, 020331 (2021).
[36] N. Sangouard, R. Dubessy, and C. Simon, Quantum repeaters based on single trapped ions, Phys. Rev. A **79**, 042340 (2009).
[37] L.-M. Duan and H. J. Kimble, Efficient engineering of multiatom entanglement through single-photon detections, Phys. Rev. Lett. **90**, 253601 (2003).
[38] X.-L. Feng, Z.-M. Zhang, X.-D. Li, S.-Q. Gong, and Z.-Z. Xu, Entangling distant atoms by interference of polarized photons, Phys. Rev. Lett. **90**, 217902 (2003).
[39] C. Simon and W. T. M. Irvine, Robust long-distance entanglement and a loophole-free Bell test with ions and photons, Phys. Rev. Lett. **91**, 110405 (2003).
[40] See Supplemental Material at [URL will be inserted by publisher] for details on the synchronization and stabilization procedures between the two nodes, a full description of our density-matrix model, an independent characterization of the noise sources, and the calculation of interference visibility, including Refs. [55–65].
[41] D. F. V. James, P. G. Kwiat, W. J. Munro, and A. G. White, Measurement of qubits, Phys. Rev. A **64**, 052312 (2001).
[42] B. Casabone, K. Friebe, B. Brandstätter, K. Schüppert, R. Blatt, and T. E. Northup, Enhanced quantum interface with collective ion-cavity coupling, Phys. Rev. Lett. **114**, 023602 (2015).
[43] T. Walker, S. V. Kashanian, T. Ward, and M. Keller, Improving the indistinguishability of single photons from an ion-cavity system, Phys. Rev. A **102**, 032616 (2020).
[44] M. Meraner, A. Mazloom, V. Krutyanskiy, V. Krcmarsky, J. Schupp, D. A. Fioretto, P. Sekatski, T. E.

Northup, N. Sangouard, and B. P. Lanyon, Indistinguishable photons from a trapped-ion quantum network node, Phys. Rev. A **102**, 052614 (2020).

[45] If photon distinguishability is due to a known frequency difference, it does not have to reduce entanglement fidelity [66]. Here, we consider distinguishability that cannot be attributed to such a frequency difference.

[46] R. Trivedi, K. A. Fischer, J. Vučković, and K. Müller, Generation of non-classical light using semiconductor quantum dots, Adv. Quantum Technol. **3**, 1900007 (2020).

[47] C. K. Hong, Z. Y. Ou, and L. Mandel, Measurement of subpicosecond time intervals between two photons by interference, Phys. Rev. Lett. **59**, 2044 (1987).

[48] D. A. Fioretto, *Towards a flexible source for indistinguishable photons based on trapped ions and cavities*, Ph.D. thesis, Leopold-Franzens-Universität Innsbruck (2020).

[49] P. Kobel, M. Breyer, and M. Köhl, Deterministic spin-photon entanglement from a trapped ion in a fiber fabry–perot cavity, npj Quantum Inf. **7**, 1 (2021).

[50] C. Ryan-Anderson, J. G. Bohnet, K. Lee, D. Gresh, A. Hankin, J. P. Gaebler, D. Francois, A. Chernoguzov, D. Lucchetti, N. C. Brown, T. M. Gatterman, S. K. Halit, K. Gilmore, J. A. Gerber, B. Neyenhuis, D. Hayes, and R. P. Stutz, Realization of real-time fault-tolerant quantum error correction, Phys. Rev. X **11**, 041058 (2021).

[51] L. Postler, S. Heuß en, I. Pogorelov, M. Rispler, T. Feldker, M. Meth, C. D. Marciniak, R. Stricker, M. Ringbauer, R. Blatt, P. Schindler, M. Mü ller, and T. Monz, Demonstration of fault-tolerant universal quantum gate operations, Nature **605**, 675 (2022).

[52] M. Zwerger, B. P. Lanyon, T. E. Northup, C. A. Muschik, W. Dür, and N. Sangouard, Quantum repeaters based on trapped ions with decoherence-free subspace encoding, Quantum Science and Technology **2**, 044001 (2017).

[53] W. J. Munro, K. Azuma, K. Tamaki, and K. Nemoto, Inside quantum repeaters, IEEE J. Sel. Top. Quantum Electron. **21**, 78 (2015).

[54] `https://doi.org/10.5281/zenodo.7031042`.

[55] C. Russo, H. G. Barros, A. Stute, F. Dubin, E. S. Phillips, T. Monz, T. E. Northup, C. Becher, T. Salzburger, H. Ritsch, P. O. Schmidt, and R. Blatt, Raman spectroscopy of a single ion coupled to a high-finesse cavity, Appl. Phys. B **95**, 205 (2009).

[56] A. Stute, B. Casabone, B. Brandstätter, D. Habicher, P. O. Schmidt, T. E. Northup, and R. Blatt, Toward an ion-photon quantum interface in an optical cavity, Appl. Phys. B **107**, 1145 (2012).

[57] K. Friebe, *On dispersive interactions between a trapped ion and a cavity field*, Ph.D. thesis, Leopold-Franzens-Universität Innsbruck (2019).

[58] J. Schupp, *Interface between trapped-ion qubits and travelling photons with close-to-optimal efficiency*, Ph.D. thesis, Leopold-Franzens-Universität Innsbruck (2021).

[59] B. Casabone, *Two ions coupled to a cavity: From an enhanced quantum computer interface towards distributed quantum computing*, Ph.D. thesis, Leopold-Franzens-Universität Innsbruck (2015).

[60] B. Casabone, A. Stute, K. Friebe, B. Brandstätter, K. Schüppert, R. Blatt, and T. E. Northup, Heralded entanglement of two ions in an optical cavity, Phys. Rev. Lett. **111**, 100505 (2013).

[61] H. Häffner, C. F. Roos, and R. Blatt, Quantum computing with trapped ions, Phys. Rep. **469**, 155 (2008).

[62] B. Efron and R. Tibshirani, *An Introduction to the Bootstrap* (Chapman & Hall, New York, 1993).

[63] A. N. Craddock, J. Hannegan, D. P. Ornelas-Huerta, J. D. Siverns, A. J. Hachtel, E. A. Goldschmidt, J. V. Porto, Q. Quraishi, and S. L. Rolston, Quantum interference between photons from an atomic ensemble and a remote atomic ion, Phys. Rev. Lett. **123**, 213601 (2019).

[64] H.-J. Briegel, B. Huttner, N. Gisin, C. Macchiavello, M. Murao, M. B. Plenio, S. Popescu, V. Vedral, P. L. Knight, W. Dür, S. J. van Enk, J. I. Cirac, and P. Zoller, Entanglement purification, in *The Physics of Quantum Information: Quantum Cryptography, Quantum Teleportation, Quantum Computation*, edited by D. Bouwmeester, A. Ekert, and A. Zeilinger (Springer Berlin Heidelberg, Berlin, Heidelberg, 2000) pp. 261–293.

[65] M. Horodecki, P. Horodecki, and R. Horodecki, General teleportation channel, singlet fraction, and quasidistillation, Phys. Rev. A **60**, 1888 (1999).

[66] G. Vittorini, D. Hucul, I. V. Inlek, C. Crocker, and C. Monroe, Entanglement of distinguishable quantum memories, Phys. Rev. A **90**, 040302 (2014).